AIMS Environmental Science

AIMS Environmental Science, 12(3): 435–460
DOI: 10.3934/environsci.2025020
Received: 27 December 2024
Revised: 28 March 2025
Accepted: 29 April 2025
Published: 26 May 2025

https://www.aimspress.com/journal/Materials

Research article

Sr(II) adsorption using amidoxime-functionalized Calcium-Alginate gel beads derived from coral skeletons: kinetic, isotherm, thermodynamic, and mechanisms studies

Alif Alfarisyi Syah, Anugrah Ricky Wijaya*, Intan Ainul Malik, and Dewinta Yuka Siwi

Department of Chemistry, Universitas Negeri Malang (UM), Jl. Semarang 5 Malang, 65145, Indonesia

* **Correspondence:** Email: anugrah.ricky.fmipa@um.ac.id.

Abstract: In this study, Ca-alginate-Amidoxime (Ca-Alg-AO) beads synthesized from coral skeleton waste and functionalized with amidoxime groups were utilized for Sr(II) adsorption in aqueous solutions. The physicochemical characterization was conducted using FTIR, TGA-DTA, SEM-EDX, and XRF. Characterization confirmed successful functionalization, as evidenced by the presence of ACN functional groups at 2251 cm^{-1}, C=N stretching vibrations at 1651 cm^{-1}, and N–O vibrations at 939 cm^{-1}, as well as thermal stability up to 282.2–652.1 °C and enhanced structural density. XRF analysis revealed an increase in Ca content from 94.63% to 94.76%, while SEM showed improved surface structural density. In aqueous solutions, the beads achieved an adsorption capacity of 13.58 mg/g and an efficiency of 84.8%, following pseudo-second-order kinetics and the Langmuir isotherm model. Thermodynamic analysis indicated an exothermic and spontaneous adsorption process driven by entropy. In seawater, the adsorption capacity decreased to 4.02 mg/g due to ion competition and Sr(II) speciation changes. Adsorption mechanisms involved ion exchange and metal-ligand complexation at lower pH levels, while higher pH promoted electrostatic interactions and complexation, with $Sr(OH)_2$ precipitation at excessive pH. Reusability tests demonstrated that the beads retained 75.7% of their initial adsorption capacity after five cycles, highlighting excellent durability and potential for environmental applications.

Keywords: coral skeleton; calcium-alginate-amidoxime; strontium; adsorption

1. Introduction

Seawater is regarded as a strategic mineral resource, especially considering the scarcity of terrestrial mineral deposits. It is estimated that seawater contains approximately 5×10^{16} tons of dissolved mineral salts, making the extraction of these resources a promising and potentially more advantageous alternative to traditional land-based mining. However, significant practical challenges remain, particularly the high costs associated with extracting metals from seawater. Thus, addressing the need for processing vast volumes of seawater and developing efficient economic systems is critical to ensuring the success of marine mineral extraction [1].

We investigate the use of cost-effective Sr(II) gel beads for the adsorption and extraction of Sr(II) from seawater. Strontium (Sr(II)) is a rare earth metal widely employed in the ceramic and glass manufacturing industries, particularly in the production of television screen glass and as an additive in ceramic ferrite magnets, among other applications in ceramic and glass products [2]. Strontium is one of the most abundant minerals in seawater, with an average concentration from 6 to 7 mg/L [3]. Nearly all strontium in seawater exists in non-radioactive forms, either as divalent cations (Sr(II)) or monovalent species ($SrOH^+$) in aqueous solutions [4]. Despite the wealth of mineral resources in seawater and the diverse industrial applications of strontium, research on the recovery of Sr(II) from seawater has been relatively limited [5,6]. Few researchers have explored methods to extract Sr(II) from seawater. Some researchers reported an extraction technique using liquid membranes [7], and successfully extracted Sr from seawater using commercial resin-based adsorbents.

The Fukushima Nuclear Power Plant disaster in 2011 caused extensive contamination of seawater with radioactive strontium (^{90}Sr), raising significant environmental and health concerns [8,9]. This isotope, a byproduct of nuclear fission, emits harmful beta-gamma radiation and possesses a relatively long half-life of approximately 29 years, enabling it to persist in marine ecosystems for extended periods [10]. The contamination has had profound implications, directly impacted marine organisms and potentially entered the food chain, thereby posing serious risks to human health. These challenges have highlighted the urgent need for the development and implementation of efficient and reliable methods to remove ^{90}Sr from seawater, which has become a critical focus of environmental remediation efforts in recent years.

The extraction of Sr(II) from seawater can be achieved through various methods, including gel beads separation, ion exchange, chemical precipitation, electrochemical techniques, and adsorption [11]. In adsorption processes, mechanisms such as chemisorption [12], ion exchange [6,11], and microprecipitation [13,14] may play a role. Researchers have increasingly focused on the ion-exchange properties of natural polysaccharides like alginic acid (ALG) [15]. For instance, calcium alginate beads have been employed to remove Cr(VI) [16] and uranium(VI) [17] from aqueous solutions. Similarly, magnetic sodium alginate beads synthesized with zirconium(VI) gel have been utilized for Pb(II) capture [18], while Ca-alginate/attapulgite clay composites have been investigated for uranium adsorption from solutions [19]. Research on Sr(II) extraction emphasizes the development of advanced beads materials with high selectivity and optimal efficiency for Sr(II) adsorption on the adsorbent surface.

Alginic acid, derived from brown seaweed, is advantageous due to its abundant availability, low cost, and high biocompatibility with living organisms [20,21]. Structurally, it is an anionic polymer

composed of 1,4-β-D-guluronate (G) and 1,4-α-L-mannonate (M) units arranged in varying sequences [22]. Alginic acid beads are commonly employed as bio sorbents for heavy metal binding, owing to their abundance of carboxyl groups capable of interacting with metal ions [23]. Although alginic acid is water-soluble, it can form insoluble hydrogels upon exposure to multivalent cations such as Ca^{2+}, Ba^{2+}, and Sr^{2+}. This gelation process, often described by the "egg-box model," involves cross-linking interactions that enhance the thermal stability and metal adsorption capacity of alginate [24,25]. In this study, coral skeletons, which consist of 90-93% calcium carbonate ($CaCO_3$), are utilized as a calcium source to facilitate this cross-linking mechanism [26].

Calcium alginate can be functionalized with chelating groups at ion exchange sites distributed throughout its matrix using a copolymerization approach [27]. Various types of chelating groups, including iminodiacetate, Schiff base, amino phosphate, and amidoxime, have been explored for this purpose [28]. Amidoxime groups, characterized by acidic (-OH) and basic ($-NH_2$) sites, exhibit a strong tendency to form stable chelate complexes with numerous heavy metal ions, particularly Sr(II) [29].

Researchers have demonstrated the efficacy of amidoxime-functionalized materials in Sr(II) adsorption [19,30]. However, all performance of adsorption is affected by amidoxime functionalization. We focus on the functionalization of amidoxime groups on Ca-alginate-AO gel beads for Sr(II) extraction from seawater, encompassing an evaluation of adsorption kinetics, thermodynamics, isotherm, capacity, and adsorbent reusability.

2. Materials and methods

2.1. Chemicals, reagents, and instrumentation

The coral skeleton waste (*Scleractinia*) used in this study was collected from Wedi Awu Beach in East Java, Indonesia. Hydrochloric acid (HCl), sodium alginate, and acetonitrile were procured from Duta Jaya Laboratory Supply (Indonesia), while glutaraldehyde was sourced from Nitrakimia Laboratory Supply (Indonesia). Additionally, 3-aminopropyl triethoxysilane (APS), potassium carbonate (K_2CO_3), and hydroxylamine hydrochloride ($NH_2OH{\cdot}HCl$) were obtained from Chemical Laboratory Supply SIP Malang (Indonesia). All reagents used were of analytical grade and were not further purified before use.

For initial characterization, Fourier Transform Infrared Spectroscopy (FT-IR, Shimadzu IR Prestige 21) was employed to identify the functional groups present in the coral and Ca-alginate-AO nanoparticles. Elemental composition was determined via X-ray Fluorescence (XRF, PANalytical X'Pert Pro), while the morphological features and composition were examined using Scanning Electron Microscopy with Energy Dispersive X-ray (SEM-EDX, FEI Inspect-S50). To evaluate the Strontium concentration in the solution, Inductively Coupled Plasma Optical Emission Spectroscopy (ICP-OES, Thermo Scientific iCAP PRO XP), and Differential Thermal Analysis (DTA/TGA/DSC, Linseis STA PT 1600) was used to investigate the thermal properties of the samples, focusing on weight changes and temperature variations.

2.2. Preparation of $CaCl_2$ from coral skeleton waste

This purification method was carried out as in research by Putra et al. (2024) [31]. The coral skeleton was cleaned by rinsing with distilled water and scrubbing to remove any impurities. Afterward, the coral was dried in an oven at 60°C for 48 hours to eliminate all moisture content. The dried coral was then finely powdered and sieved through a stainless-steel mesh with a 200-mesh size. The resulting powder was subjected to calcination at 800°C for 2 hours and left to cool to ambient temperature. A 0.5 M $CaCl_2$ solution was prepared by reacting 100 mL of 1 M HCl solution with the calcium extracted from the coral skeleton. This mixture was stirred for 3 hours at 40°C on a hotplate with a magnetic stirrer to ensure thorough homogenization. Finally, the solution was filtered to separate the liquid from the solid residue.

2.3. Preparation of Ca-Alg-AO

Sodium alginate was dissolved in distilled water at a concentration of 1%, and the dissolution was facilitated using a mechanical stirrer set to 700 rpm to ensure thorough mixing. Once the sodium alginate was dissolved, it was carefully added dropwise to a 0.5 M calcium chloride ($CaCl_2$) solution. The resulting calcium alginate (Ca-Alg) mixture was left to immerse for 45 minutes to ensure proper gel formation and then subjected to filtration to separate the gel beads. These beads were washed rigorously with distilled water, repeating the washing process eight times to remove any residual impurities or unreacted chemicals. In the next phase of synthesis, 5 grams of the Ca-Alg microspheres were dispersed into 100 mL of ethanol. To this suspension, 5 mL of 3-aminopropyl triethoxysilane (APS) was added, and the mixture was subjected to a reflux process at 70°C for 6 hours to facilitate the covalent bonding between the APS and the alginate beads. After the reaction, the microspheres were thoroughly washed with distilled water and ethanol to remove any unreacted APS and other residual chemicals. The microspheres were then dried under vacuum at 60°C for 2 hours to remove any remaining solvent and water.

Following the synthesis of the Ca-Alg-APS gel beads, the aldehyde group activation process commenced by immersing the beads in a solution of 5 mL glutaraldehyde and 100 mL ethanol at room temperature. This mixture was stirred for 6 hours to enable the interaction between the amine groups on APS and the glutaraldehyde molecules, forming a stable crosslinked structure. After the reaction, the product was washed again with distilled water and ethanol to remove any unreacted reagents, and then dried in an oven at 60°C. The next step involved soaking the Ca-Alg-APS-Glu beads in a solution of 30 mL acetonitrile (ACN) dissolved in 100 mL ethanol at 10°C for 6 hours to promote the formation of nitrile chelating groups on the membrane surface. The nitrile groups were crucial for enhancing the metal-binding capacity of the beads. The product was then thoroughly rinsed and dried before being treated with a solution containing 2.0 g of K_2CO_3 and 2.0 g of $NH_2OH{\cdot}HCl$ dissolved in 100 mL ethanol. This treatment was conducted for 6 hours at 70°C in a closed flask to facilitate the amidoxime functionalization of the calcium alginate beads. Following this step, the final product, Ca-Alg–amidoxime (AO), was washed extensively with distilled water and ethanol to remove any residual chemicals. Finally, the beads were dried under vacuum conditions at 60°C to obtain the purified Ca-Alg-AO product.

2.4. Characterization of $CaCO_3$, Ca-Alg, Ca-Alg-ACN, and Ca-Alg-AO gel beads

Initial characterization of $CaCO_3$, Ca-Alg, Ca-Alg-ACN, and C-aAlg-AO gel beads was performed using XRF to non-destructively assess elemental composition of coral skeleton. FT-IR was employed to identify functional groups present in the compounds. SEM-EDX was utilized to analyze emitted X-rays, yielding insights into elemental composition and structural morphology. TGA/DTA was conducted to evaluate thermal properties by measuring weight changes and temperature variations.

2.5. Adsorption and reusability experiment

Strontium adsorption was investigated through batch experiments. Initially, 0.025 g of adsorbent was placed into separate Erlenmeyer flasks. Subsequently, 20 mL of a 20 mg L^{-1} Sr^{2+} chloride solution was added to each flask, with several dose and pH variations. These Erlenmeyer flasks were then stirred at 120 rpm for 30 minutes at room temperature. The primary objective of this experiment was to determine the optimal dose and pH values required for effective Strontium adsorption.

To determine the ideal contact time and concentration between the adsorbent and adsorbate, contact time variations were started, ranging from 10 to 120 minutes and at concentration variations starting from 5 to 50 mg L^{-1}. Following this, the solution was filtered using Whatman 42 filter paper. The filtered samples were analyzed to determine the Strontium concentration using ICP-OES. Additionally, temperature effects were assessed using the batch method, with temperature variations set at 27, 30, 40, and 50°C, while maintaining the optimal pH and contact time.

$$\text{Adsorption \%} = \frac{Co-Ce}{Co} \text{ x } 100 \tag{1}$$

$$q_e = \frac{(Co-Ce)\ x\ V}{m} \tag{2}$$

q_e (mg g^{-1}) shows the adsorption capacity, *C*o (mg L^{-1}) and *C*e (mg L^{-1}) show the Strontium concentration before and after the adsorption process, m (g) and V (L) show the amount of adsorbent, and the volume of the solution, respectively. Reusability experiments for Sr(II) were carried out using a 1M HNO. Ca-Alg-AO microspheres, which had previously adsorbed Sr(II), were first rinsed and then dried at 60°C before being utilized in the desorption tests. Similar to the Sr(II) adsorption procedure, 0.25 g of Ca-Alg-AO microspheres was introduced into 0.02 L of each regenerant solution for contact time of 30 minutes.

2.6. Adsorption kinetics

To determine the most effective kinetic model, the data for the batch adsorption study were studied via pseudo-first order, and pseudo-second order, as indicated by Equations 3&4, respectively.

$$\textit{Pseudo-first-order}: \log(q_{e-}\ q_t\ ) = \log q_{e-}\ \frac{k_1 t}{2.303} \tag{3}$$

$$\textit{Pseudo-second-order}: \frac{t}{q_t} = \frac{1}{K_2\, q_e^2} + \frac{1}{q_e} \tag{4}$$

q_t (mg g^{-1}) and q_e (mg g^{-1}) refer to the quantity of Sr(II) absorbed at a given time and the equilibrium optimum, respectively. In the context of Pseudo-first-order and Pseudo-second-order

kinetic equations, k_1 (min^{-1}) and k_2 (g/mg·min) represent the rate constants. Determination of the rate constants k_1 and k_2, involves analyzing the gradient of the natural logarithm (q_e - q_t) against time (t).

The intra-particle diffusion model was also calculated using the Weber-Morris equation [32]:

$$q_t = k_p \text{ x } t^{0.5} + C \tag{5}$$

q_t represents the amount of adsorbate adsorbed at time t (mg.g), k_p denotes the intra-particle diffusion rate constant (mg/g-$min^{0.5}$), $t^{0.5}$ refers the square root of time ($min^{0.5}$) and *C* corresponds to the boundary layer thickness (mg/g). When the plot of q_t vs $t^{0.5}$ forms a a straight line passing through the origin, intra-particle diffusion is the sole controlling mechanism. However, if the plot exhibits multiple linear segments, this suggests the involvement of multiple adsorption mechanisms, such as film diffusion, pore diffusion, and surface adsorption. Finally, a larger *C* value indicates a greater boundary layer effect, implying that external mass transfer plays a significant role.

2.7. Adsorption isotherm

The Langmuir, Freundlich, and Temkin models were used for the study of isotherms fitting on the adsorption data, as shown in Eqs 6 and 7, respectively

Freundlich isotherm model equation: $\log_{q_e} = \log K_{f+} \frac{1}{n} log C_e$ (6)

Langmuir isotherm model equation: $\frac{C_e}{q_e} = \frac{1}{K_L\ q_m} + \frac{C_e}{q_m}$ (7)

In the equation, q_m (mg g^{-1}) represents the maximum monolayer adsorption capacity, while q_e (mg g^{-1}) is the amount of Sr(II) adsorbed per unit mass of adsorbent. C_e (mg L^{-1}) indicates the final concentration of strontium ions in solution, and C_o (mg L^{-1}) is the initial concentration of Sr(II) ions. K_L (l/mg) is the Langmuir constant related to the adsorption energy, and K_f (mg g^{-1}) together with 1/n (l/g) are related to the adsorption capacity of the sorbent and the intensity of the adsorption process (heterogeneity parameter).

2.8. Thermodynamic studies

Thermodynamic parameters (ΔH, ΔS, ΔG) are derived from Equations (8) and (9) to explain the randomness, spontaneity, and nature of the sorption process:

$$K_L = \frac{C_a}{C_s}$$

van't Hoff model equation: $ln\ k_L = \frac{\Delta S^O}{R} + \frac{\Delta H^O}{RT}$ (8)

$$\Delta G^O = -RTln\ k_L \tag{9}$$

where R (8.31 J mol^{-1} K^{-1}) universal gas constant, T temperature in Kelvin, and k_d (m^3

mol^{-1}) concentration of adsorbate to the adsorbent ratio in equilibrium. The Van't-Hoff plot's slope and intercept of ln k_d as a function of 1/T x 10^3, from which $\Delta H°$ and $\Delta S°$ were acquired.

3. Results and discussion

3.1. Chemical characterization of adsorbents

3.1.1. Chemical competition analysis

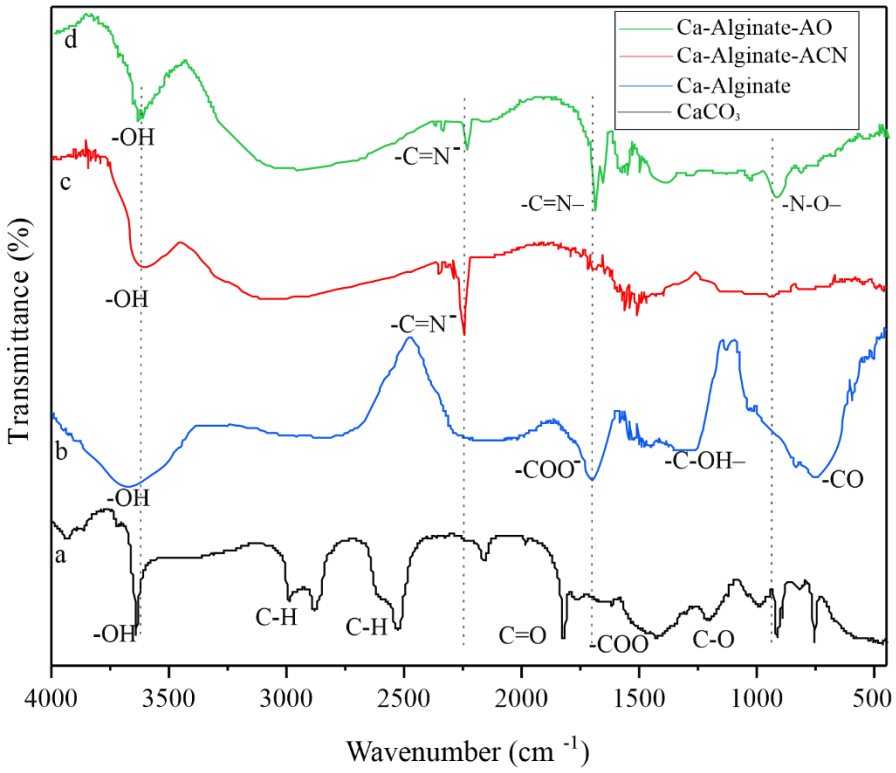

Figure 1. (a) $CaCO_3$, (b) Ca-Alg, (c) Ca-Alg -ACN, and (d) Ca-Alg-AO

The FT-IR spectra of Ca-Alg, Ca-Alg-ACN, and CaAlg-AO reveal significant modifications resulting from the incorporation of amidoxime functional groups. Notably, the distinct peak at 751.06 cm^{-1} (Figure 1a) corresponds to Ca-O vibrations associated with calcium oxide (CaO) [12,18], reflecting the structural integrity of the calcium alginate matrix and indicating effective cross-linking and stabilization via calcium interactions. Furthermore, the absorption band at 2251 cm^{-1} signifies the successful integration of ACN chains on the surface of cross-linked Ca-alginate microspheres, marked by the diagnostic –C≡N band (Figure 1b) [33]. The reduction in C≡N peak intensity (Figure 2c) following the addition of H_2N–C=N–OH groups suggest active participation of C≡N groups in chemical interactions, leading to spectral modifications. In Ca-alginate-AO, new absorption peaks characteristic of amidoxime groups emerge; specifically, the band at 1651 cm^{-1} is assigned to C=N stretching, while a peak at 939 cm^{-1} corresponds to N–O vibration [27].

3.1.2. Thermal properties

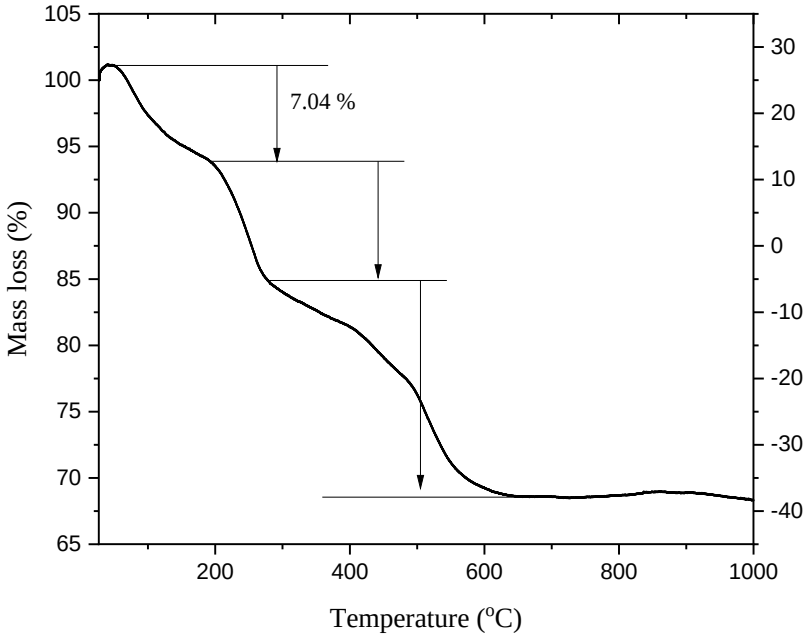

Figure 2. Curve analysis TGA of Ca-Alg-AO.

The TGA thermal analysis of Ca-alginate-AO beads in Figure 3 reveals three stages of thermal degradation in the polymer granules. The initial stage occurs within the temperature range of 27 to 193.1 °C, showing a weight loss of 9.7%, which is attributed to the evaporation of water molecules trapped within the structural network [34]. The second and third stages, observed between 193.2 and 282.2 °C, are associated with partial degradation of sodium alginate, leading to the breaking of some molecular chains. The final degradation stage occurs within the range of 282.2 to 652.1 °C, where chain scission, fragment formation, and monomer release take place, resulting in a weight loss of 17.1% [34,35].

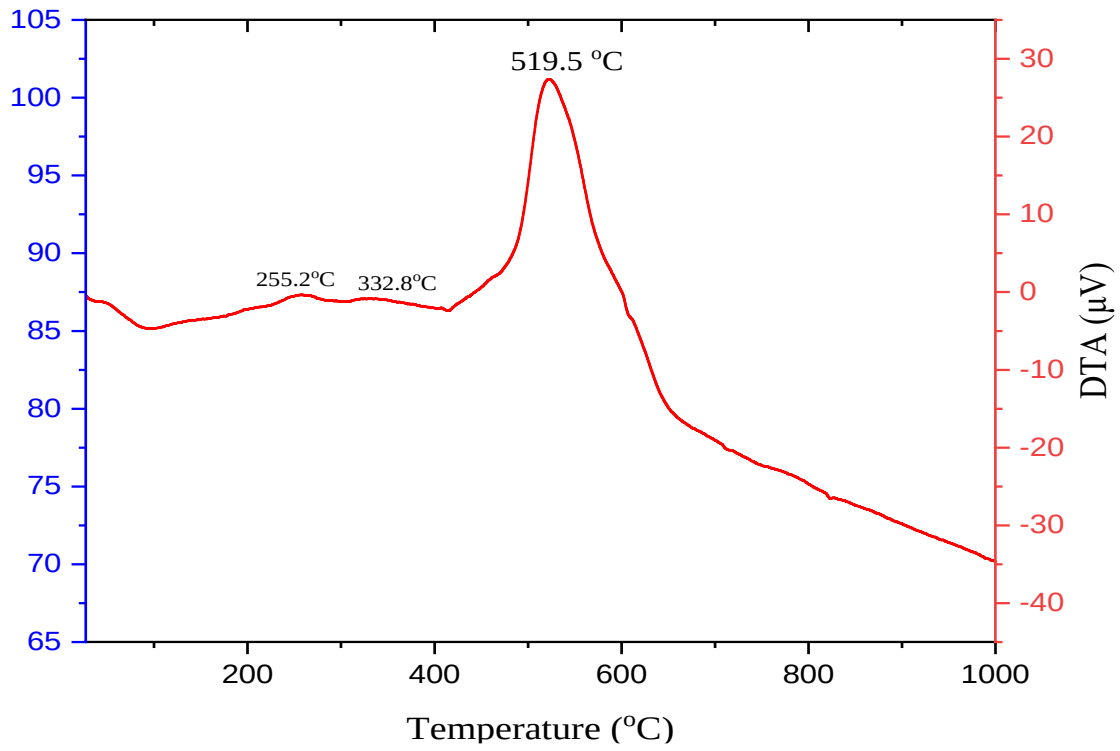

Figure 3. Curve analysis DTA of Ca-Alg-AO.

The DTA results (Figure 3) provide a detailed thermal profile that aligns closely with the corresponding TGA data, revealing significant insights into the thermal behavior of the Ca-alginate-AO membrane granules. The initial endothermic peak observed at approximately 100°C [36] reflects the energy required to evaporate water that is physically adsorbed on the surface and within the pores of the membrane [37]. This indicates that the material retains moisture even after the drying process, a characteristic typical of hydrophilic materials like alginate-based polymers. Following the dehydration stage, two distinct exothermic peaks are observed at 255.2°C and 332.8°C. These peaks represent the combustion of organic components within the membrane structure, such as residual alginate and functional groups introduced during the amidoxime functionalization [38]. The exothermic reactions at these temperatures correspond to the release of energy as the organic matter oxidizes, which is further corroborated by a simultaneous weight loss observed in the TGA profile. This suggests that the material contains thermally unstable groups, likely derived from the functionalization process, that decompose in this temperature range [39].

An additional exothermic peak is detected at 519.5°C, which marks the thermal degradation of the molecular side chains within the Ca-alginate-AO structure. This peak indicates a more stable thermal region associated with the backbone of the polymer. The high degradation temperature reflects the robust crosslinked network formed by the interactions between calcium ions, alginate, and amidoxime functional groups [36]. The presence of such a peak underscore the structural integrity and thermal stability imparted by the crosslinking and functionalization processes. Further analysis of the DTA curve reveals a gradual baseline shift, which suggests minor thermal events occurring beyond 520°C. This behavior is indicative of the slow degradation of residual inorganic or mineral content, likely originating from calcium carbonate remnants in the alginate structure [40]. The TGA profile

supports this observation by showing a final weight plateau after this temperature, suggesting that the material stabilizes thermally with only minor residue remaining, primarily composed of inorganic components [38] .

3.1.3. The composition of properties

Table 1. XRF analysis results of coral skeleton powder before alcination.

Unsur	Wt (%)	Oxide	Wt (%)
Ca	93.65	CaO	94.63
Fe	0.30	Fe_2O_3	0.29
Zn	0.038	ZnO	0,035
Sr	4.74	SrO	3.73
Mo	0.98	MoO_3	1.20
Lu	0.20	Lu_2O_3	0.16
Zr	0.09		

Tabel 2. XRF analysis results of coral skeleton powder after Calcination.

Element	Wt (%)	Oxide	Wt (%)
Ca	93.85	CaO	94.76
Fe	0.44	Fe_2O_3	0.43
Ti	0.061	TiO_2	0.069
Sr	4.68	SrO	3.68
Mo	0.71	MoO_3	0.87
Lu	0.21	Lu_2O_3	0.16
Cu	0.044	CuO	0.037

The XRF characterization results are summarized in Table 1, which shows that the coral skeleton before calcination contains 94.63% Ca in the form of $CaCO_3$. Table 2 shows that the percentage of CaO after calcination increases to 94.76%. These results confirm that the CaO content in the coral skeleton rises after calcination. This increase in Ca percentage is attributed to calcination, a thermal decomposition process designed to eliminate organic compounds or other gases present in the sample [26]. All other components are considered impurities, resulting from natural sources, with a combined composition totaling less than 5%.

3.1.4. Surfaces properties

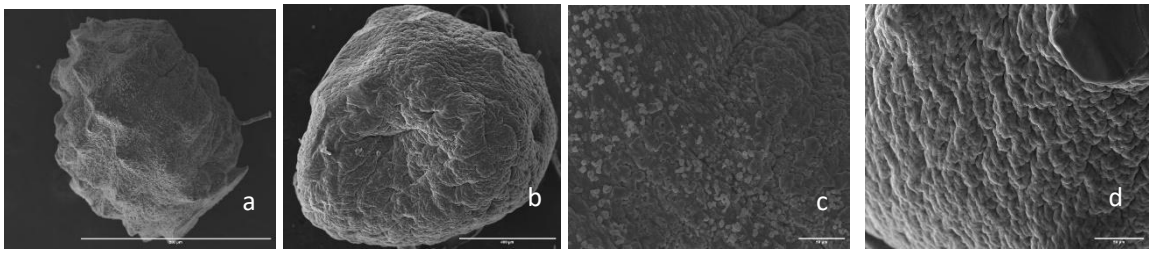

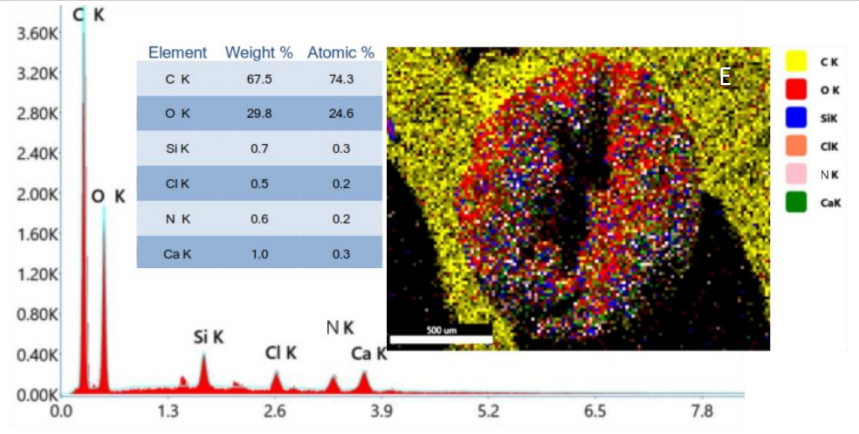

Figure 4. SEM photographs of monomer-non imprinted (a) and imprinted (b) alginate microspheres. Surface structure of (c) Ca-Alg, (d) Ca-Alg-AO, and EDS of (e) CaAlg-AO.

The surface morphology of natural, non-imprinted, and imprinted cross-linked alginate polymers was investigated using scanning electron microscopy (SEM) (Figures 4a,b). All samples displayed a spherical morphology, with the imprinted cross-linked alginate microspheres exhibiting relatively larger dimensions. This increase can be attributed to the integration of modified active polymer chains that are grafted onto the surface of the cross-linked alginate. Furthermore, the analysis aimed to elucidate the homogeneity and microstructure of the Ca-alginate-AO beads, as depicted in Figures 4c,d. Figure 4d illustrates uniformly sized microspheres that are evenly distributed across the alginate surface. This uniformity is likely a result of the carboxyl groups (COO−) present in alginate, which can engage in interactions and form long chains with amino groups (NH_3^+), aldehydes (-CHO), nitriles (-CN), and amidoximes (-OH & -NH_2) found in the Ca-alginate-AO microspheres, which is supported by EDS data in Figure 4e [2,16,20]. Additionally, the morphological characteristics of these material granules are primarily influenced by the original microstructure of the Ca-alginate (Figure 3b), with an observed increase in structural density at specific interfaces. In the foreseeable future, BET (Brunauer-Emmett-Teller) analysis is recommended for estimating the specific surface area of porous materials available for adsorption.

3.2. Adsorption performance in batch experiments

3.2.1. Optimization of adsorbent dose and effect of pH on Sr(II) adsorption

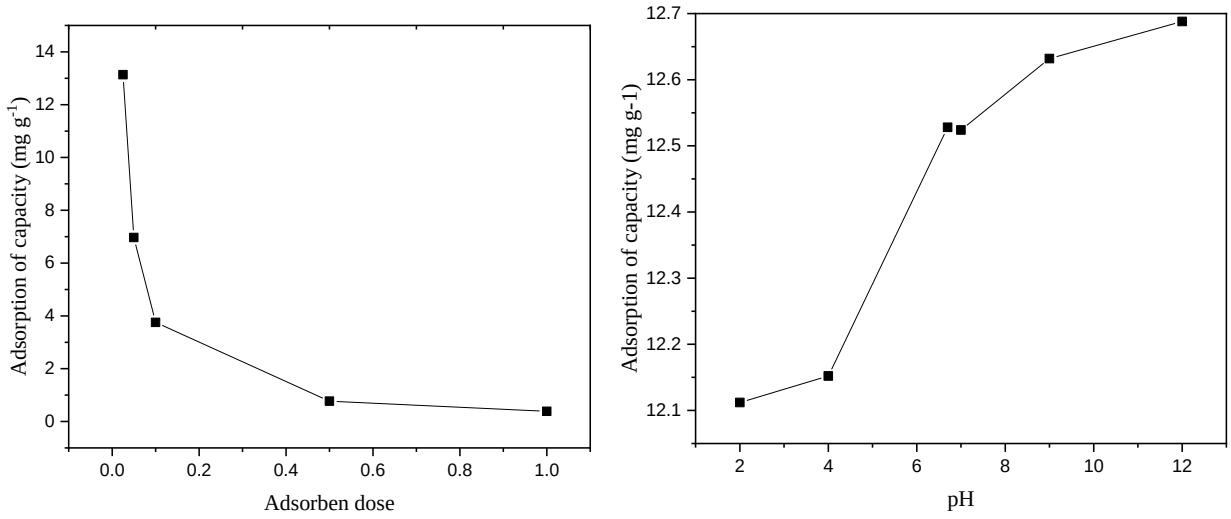

Figure 5. Effect of adsorbent dose and solution pH on Sr(II) adsorption on CaAlg-AO beads ([Sr(II)]: 20 mg/L; adsorbent: 0.025 g; solution volume: 0.02 L; reaction time: 30 min; reaction temperature: 27°C, 130 rpm).

Figure 5 shows the optimization of adsorbent dose and pH plays a crucial role in determining the adsorption efficiency of Sr(II) ions on Ca-Alg-AO. The relationship between the amount of adsorbent and adsorption capacity (mg/g) demonstrates a trend were lower doses of adsorbent yield higher adsorption capacities. At an adsorbent dose of 0.025 g, the adsorption capacity reaches a maximum of 13.13 mg/g, which decreases significantly to 0.39 mg/g at 1 g. This decline can be attributed to two factors. First, increasing the amount of adsorbent results in a more dispersed distribution of Sr(II) ions across the adsorbent, reducing the adsorption capacity per unit mass. Second, higher doses of adsorbent lead to overlapping active sites on the adsorbent surface, thereby diminishing the availability of these sites for Sr(II) ions. Consequently, lower amounts of adsorbent exhibit higher adsorption efficiency, though the total Sr(II) adsorption may be lower. Optimizing the adsorbent dose is critical for achieving efficient adsorption while maintaining practical applicability.

Our results using Ca-Alg-AO demonstrated an adsorption capacity of 13.13 mg/g (at a dose of 0.025 g), corresponding to a net adsorption of 525.5 mg/g. For comparison, this performance is more efficient than that reported in a study where a Sr(II) adsorption capacity of 360.23 mg/g was achieved using a PSi/AOX adsorbent [41]. Additionally, some studies employing Ca/alginate and AO-APEI adsorbents [30] reported Sr(II) adsorption capacities of 110.0 mg/g and 189.0 mg/g, respectively. These findings highlight the enhanced adsorption efficiency associated with the combination of coral skeleton amidoxime functionalization.

The adsorption capacity of Sr^{2+} ions by the Ca-Alg-AO adsorbent demonstrates a notable increase with rising pH, ranging from 12.112 mg/K at pH 2 to a peak value of 12.688 mg/K at pH 12. This trend is closely linked to alterations in the surface chemistry of the adsorbent and the speciation behavior of Sr^{2+} ions under varying pH conditions. At lower pH levels (2–4), the high concentration of H^+ ions promote the protonation of functional groups on the adsorbent surface, such as carboxylate ($-COO^-$) and amidoxime (-C=NOH). This protonation diminishes the negative charge density on the surface, reducing electrostatic attraction toward the positively charged Sr^{2+} ions. Additionally, the high abundance of H^+ ions compete with Sr^{2+} for available adsorption sites, resulting in a lower adsorption

capacity. At neutral to alkaline pH levels (6.7–12), the adsorption capacity significantly improves as the functional groups on the adsorbent undergo deprotonation, increasing the surface's negative charge. This facilitates stronger electrostatic interactions and specific complexation between Sr^{2+} ions and the adsorbent's active sites. The continuous rise in adsorption capacity, reaching its maximum at pH 12, indicates that electrostatic forces and coordination interactions dominate the adsorption mechanism in this pH range. Moreover, at higher pH, the formation of $Sr(OH)^{+}$ species may enhance adsorption, although this is accompanied by a growing likelihood of $Sr(OH)_2$ precipitation. Precipitation can reduce the concentration of free Sr^{2+} ions in solution, thereby limiting the overall adsorption efficiency

3.2.2. Adsorption kinetic

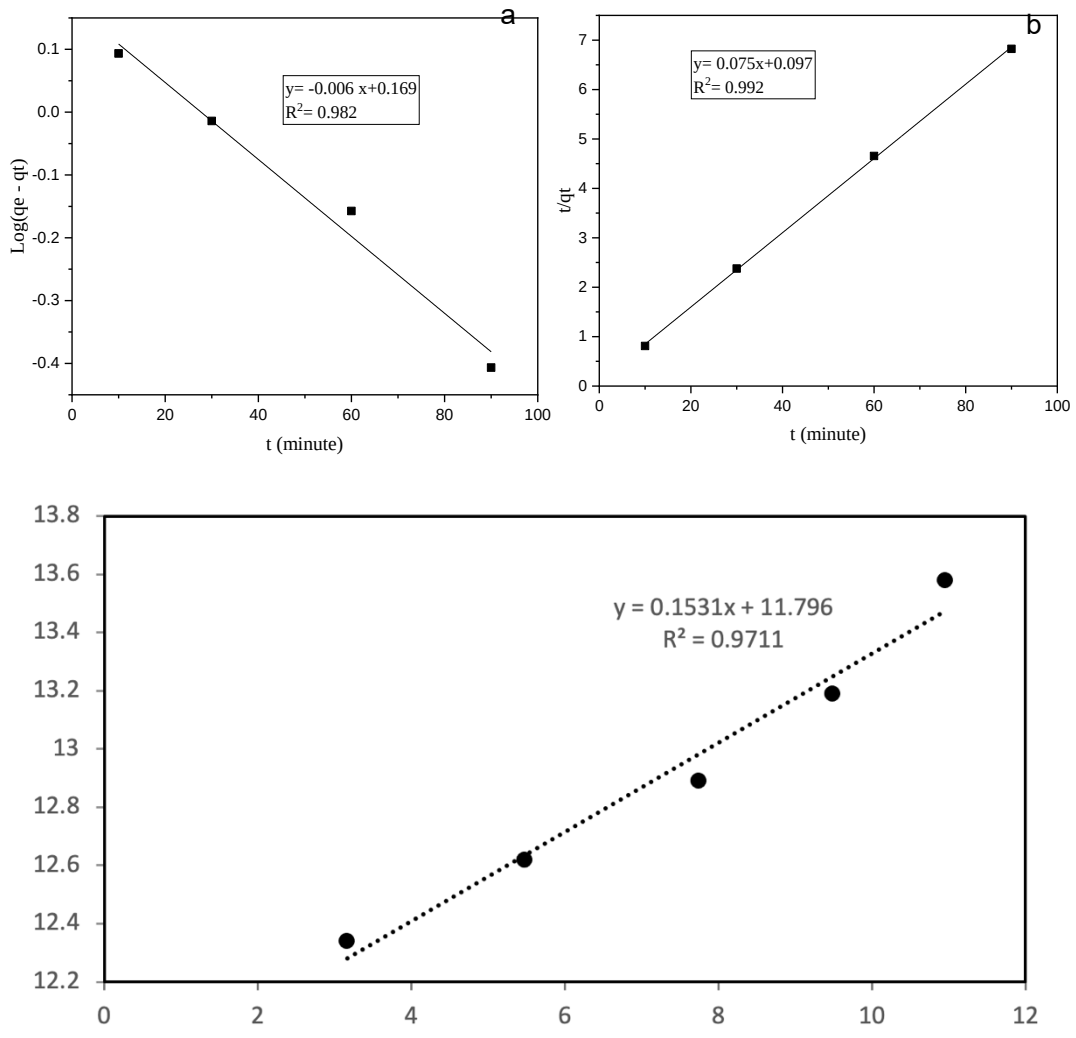

Figure 6. *Pseudo-first-order* (a) and *pseudo-second-order* (b) kinetic of Sr^{2+} ions on CaAlg-AO beads (m: 0.025 g; T: 300 K; pH: 4.00; C_o: 20 mg L^{-1}; V: 20 ml), (c) Intra-particle diffusion model.

Table 3. Kinetic parameters and results of Sr^{2+} adsorption experiments with a contact time range of 10-120 minutes.

t (minute)	C_t (mg L^{-1})	q_t (mg g^{-1})	Log (q_e - q_t)	t/ q_t
10	4.57	12.34	0.093	0.810
30	4.23	12.62	-0.014	0.793
60	3.89	12.89	-0.157	0.776
90	3.51	13.19	-0.407	0.758
120	3.02	13.58	-	0.736

Pseudo-First-Order		Pseudo-Second-Order	
$q_{e.exp}$	13.58	$q_{e.cal}$	13.30
$q_{e.cal}$	1.47	K_2	1821.49
K_1	0.001	R^2	0.992
R^2	0.982		

Intra-particle diffusion model	
k_p = 0.153	C = 11.796

Based on Figure 6 and Table 3, the adsorption kinetics of Sr^{2+} ions onto the CaAlg-AO material exhibit a better fit to the pseudo-second-order model compared to the pseudo-first-order model, as indicated by the higher coefficient of determination (R^2) for the pseudo-second-order model (0.992) compared to that of the pseudo-first-order model (0.982). The pseudo-second-order model is more suitable because it describes chemisorption mechanisms, involving chemical bond formation or electron transfer between Sr^{2+} ions as the adsorbate and the CaAlg-AO surface as the adsorbent. In contrast, the pseudo-first-order model, which primarily represents physisorption governed by van der Waals forces, is less applicable for this system [30,42].

The experiment adsorption capacity ($q_{e.exp}$ = 13.58 mg/g) is closely aligned with the theoretical adsorption capacity derived from the pseudo-second-order model (q_e = 13.30 mg/g), whereas the pseudo-first-order model significantly underestimates the capacity (q_e = 1.47 mg/g), further confirming the inadequacy of the pseudo-first-order model for this system. Additionally, the pseudo-second-order rate constant (K_2 = 1821.49 m mg^{-1} min^{-1}) is substantially higher than the pseudo-first-order rate constant (K_1 = 0.001 min^{-1}), reflecting a much faster reaction rate and higher adsorption efficiency under the pseudo-second-order mechanism. The linear increase of $1/q_t$ over time, as illustrated in Figure 6b, further validates the appropriateness of the pseudo-second-order model. In contrast, the decline of log(q_e - q_t) in the pseudo-first-order model (Figure 6a) does not consistently align with the experimental data. These findings suggest that the adsorption of Sr^{2+} ions onto Ca-Alg-AO is predominantly governed by a pseudo-second-order kinetic mechanism, which reflects the chemical nature of the adsorption process. This also implies that Sr^{2+} ions are likely adsorbed onto the active sites of the material through strong chemical interactions, resulting in efficient adsorption behavior that adheres to the pseudo-second-order model [6,13]. In addition, intra-particle diffusion modeling was applied to investigate the surface effect. As shown in Fig. 6c and Table 3, the linear plot of q_t vs

$t^{0.5}$ indicates that the adsorption process is controlled by intra-particle diffusion. The Ca-Alg-AO adsorbs Sr(II) through a single adsorption mechanism involving film diffusion, pore diffusion, and surface adsorption. The high *C* value (11.976) suggests a pronounced boundary layer effect, indicating that external mass transfer plays a significant role in the interaction between Ca-Alg-AO and Sr(II).

3.2.3. Adsorption isotherm

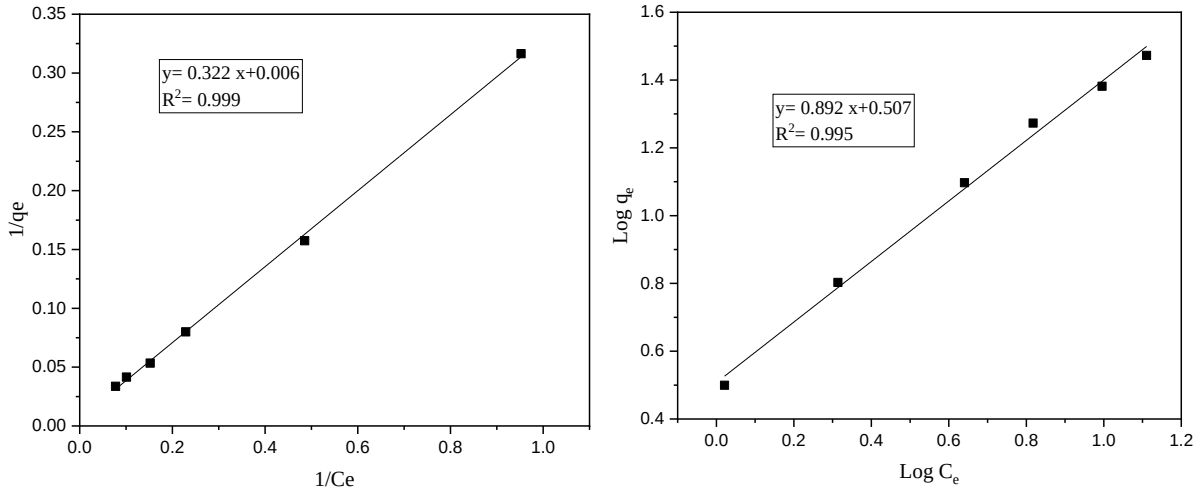

Figure 7. *Langmuir* (a) and *Freundlich* (b) sorption isotherm of Sr^{2+} ions on CaAlg-AO beads (m: 0.025 g; T: 300 K; pH: 4.00; t: 30 min; V: 20 ml).

Table 4. Isotherm parameters and results of Sr^{2+} adsorption experiments at various concentrations.

C_o mg L^{-1}	C_e (mg L^{-1})	q_e (mg g^{-1})	$1/q_e$	$1/C_e$	Log C_e	Log q_e
5	1.05	3.16	0.952	0.316	0.021	0.500
10	2.06	6.35	0.485	0.157	0.314	0.803
20	4.37	12.50	0.229	0.080	0.640	1.097
30	6.57	18.74	0.152	0.053	0.818	1.273
40	9.9	24.08	0.101	0.042	0.996	1.382
50	12.9	29.68	0.078	0.034	1.111	1.472
Isotherm Langmuir						
q_{max} (mg/g)			3.098			
K_L (L/mg)			0.9998			
Isotherm Freundlich						
n			0.897			
K_f (mg/g)			0.274			

The adsorption characteristics of Sr^{2+} ions onto Ca-Alg-AO beads were analyzed using the Langmuir and Freundlich isotherm models to elucidate the underlying adsorption mechanism and evaluate the adsorbent's performance. The Langmuir isotherm, which assumes monolayer adsorption on a surface with homogeneously distributed and energetically equivalent active sites, provides a maximum adsorption capacity (q_{max}) of 3.098 mg g^{-1}. This value demonstrates a moderate binding

capacity, rendering the material suitable for practical applications while highlighting the potential for further optimization to enhance performance. The Langmuir constant (KL) is -0.006 mg L^{-1}, suggesting weak interactions between Sr^{2+} ions and the adsorbent. These weak interactions are likely dominated by physical adsorption processes mediated is electrostatic forces [43]. Moreover, the coefficient of determination (R^2) for the Langmuir model is exceptionally high at 0.999, affirming the suitability of the model and indicating that the adsorption behavior is consistent with a monolayer adsorption mechanism on a uniform surface [44,45].

Complementary insights are obtained from the Freundlich isotherm, which describes multilayer adsorption on heterogeneous surfaces. The Freundlich constant (K_f) of 0.274 mg g^{-1}suggests limited adsorption capacity at low Sr^{2+} concentrations, reflecting reduced efficiency in dilute solutions. The Freundlich exponent is calculated as 0.897, indicating non-ideal adsorption behavior, as adsorption sites likely exhibit varying energetic favorability. It is worth noting that n>1 typically signifies favorable adsorption, whereas n<1, as observed in this study, implies diminished adsorption favorability [46]. The R^2 value for the Freundlich model, while slightly lower at 0.995 compared to the Langmuir model, demonstrates a strong correlation, confirming its applicability to the system. However, the slightly reduced precision of the Freundlich model suggests that it may be less suitable for describing the adsorption mechanism of Sr^{2+} ions onto Ca-Alg-AO beads compared to the Langmuir model [30,43,47].

3.2.4. Thermodynamic studies

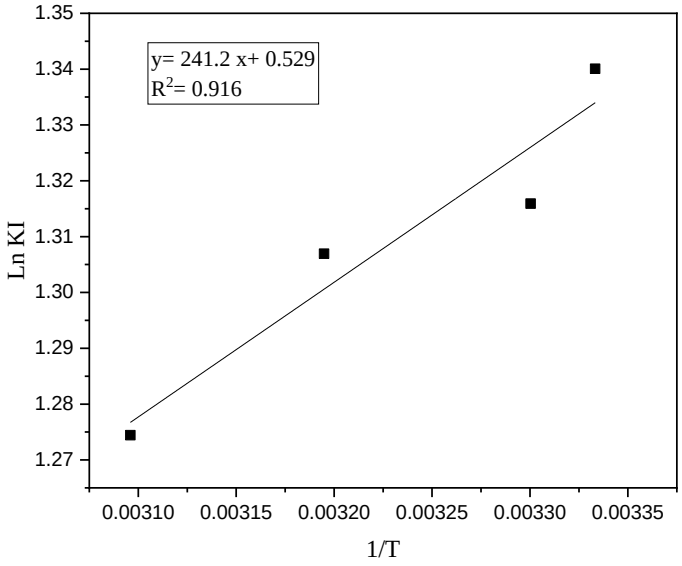

Figure 8. Van't-Hoff's plot for adsorption of Sr(II) using Ca-Alg-AO.

Table 5. Thermodynamic parameters for the adsorption of Sr(II) Ca-Alg-AO.

T (K)	ΔH (kJ mol^{-1})	ΔS (kJ mol^{-1} K^{-1})	ΔG (kJ mol^{-1})
300.15	-2.005	4.404	-3.327
303.15			-3.340
313.15			-3.384
323.15			-3.429

Thermodynamic analysis employing Van't Hoff plots and associated parameters offers valuable insights into the mechanism and spontaneity of Sr^{2+} adsorption onto Ca-Alg-AO beads. The ΔG negative values across the examined temperatures unequivocally confirm the spontaneous nature of the adsorption process. Especially, the increasingly negative ΔG values with rising temperature signify enhanced thermodynamic favorability, driven primarily by an entropy-dominated mechanism (- TΔ*S*) [48–50]. The enthalpy change (ΔH) of -2.005 kJ/mol indicates an exothermic process, suggesting that the adsorption is predominantly governed by physical interactions such as Van der Waals forces. Furthermore, the positive entropy change (ΔS) of 4.404 J/mol·K reflects increased system disorder, likely attributed to the desolvation of Sr^{2+} ions and the reorganization of water molecules within the adsorbent's microenvironment during the adsorption process [41,50].

Despite the greater thermodynamic favorability indicated by more negative ΔG values at elevated temperatures, the adsorption capacity (q_e) exhibits a slight decline with increasing temperature, decreasing from 12.680 mg/g at 300.15 K to 12.504 mg/g at 323.15 K. This trend aligns with the exothermic nature of the adsorption process, wherein higher temperatures disrupt the adsorbate-adsorbent interactions, thereby promoting desorption. This observation highlights a fundamental thermodynamic, and while elevated temperatures enhance spontaneity, they simultaneously reduce the adsorption efficiency due to the weakening of adsorptive forces [11,51].

3.2.5. Application in seawater and suggested mechanisms for adsorption Sr(II) ion on Ca-Alg-AO

The seawater used in this study was taken from the southern coastal waters of Malang Beach, namely Wedi Awu. Evaluation of the performance of the Ca-Alg-AO adsorbent in the adsorption of Sr(II) was carried out at three pH conditions, namely the pH at the sampling location and at pH 9 and 12. Seawater samples were tested for levels using ICP-OES and the original concentration of strontium in seawater without treatment was 8.16 mg/L. This is similar to the XRF results (Table 1) where there is also strontium content in coral skeletons. Sr in seawater can be influenced by the dynamics of ocean circulation, can be caused by geochemical factors and upwelling processes, where mineral-rich seawater from the seabed rises to the surface. In this application of strontium adsorption in seawater, various optimum conditions obtained previously were used.

Table 6. Application of Sr(II) adsorption in seawater by CaAlg-AO beads (m: 0.025 g; T: 300.15 K; t: 120 min ; V: 20 ml).

pH	Condition of native seawater Sr(II) (mg L^{-1})	Ce (mg L^{-1})	Adsorption (%)	Capacity of adsorption (mg/g)
6.8	8.16	3.90	52.20	3.41
9	8.16	3.60	55.88	3.65
12	8.16	3.14	61.52	4.02

Based on Table 6, at pH 12, the adsorption capacity of Ca-Alg-AO for Sr(II) in seawater is the highest compared to pH 6.8 and 9. This can be caused by Sr(II) speciation changes at high pH (e.g., formation of $Sr(OH)^+$), the greater deprotonation of the adsorbent compensates for this effect, enabling efficient adsorption. Furthermore, the decrease in adsorption capacity of Ca-Alg-AO for Sr(II) in seawater 4.02 mg/g is mainly due to competition from other ions and changes in Sr(II) speciation at

pH 12. Seawater contains high concentrations of competing cations, which can occupy adsorption sites on the adsorbent like Cl^-, SO_4^{2-}, and in particular, ions like Ca^{2+} and Mg^{2+}, which have similar ionic radii and charges to Sr^{2+}. The strontium in aqueous solution was found as Sr^{2+} ions and $SrOH^+$ species on a broad pH interval (pH 6–10), but $SrOH^+$ was the main form at pH > 12.8 [52]. The strontium ions removal capacity at pH >7 may be due to a combined effect of adsorption and precipitation on the activated carbon surface [53].

By reinforcing the findings obtained from the chemical characterization of the Ca-Alg-AO adsorbent surface and the adsorption capacity of Sr^{2+} ions as a function of solution pH, a plausible adsorption mechanism can be proposed. At low pH (pH < 4), competition between H^+ ions and Me^{2+} ions for the active sites of the adsorbent becomes dominant. This is attributed to the protonation of active functional groups such as amidoxime (-C=NOH) and carboxylate ($-COO^-$) on the adsorbent surface, which reduces the availability of negatively charged sites for interaction with Sr^{2+} ions. Generally, at pH below the pKa of the carboxylate group, Sr^{2+} adsorption on Ca-Alg-AO can occur via the formation of coordination complexes between the oxygen atoms of the carboxylate or amidoxime groups and the Sr^{2+} ions, even though electrostatic interactions are weakened due to the positively charged adsorbent surface [54].

At higher pH levels, the active groups on the adsorbent surface begin to deprotonate, increasing the negative surface charge and enhancing electrostatic interactions with Sr^{2+} ions. Moreover, the formation of coordination bonds between metal ions and the functional groups strengthens, resulting in higher adsorption efficiency. This mechanism may also involve ion exchange, where Sr^{2+} ions replace Ca^{2+} or H^+ ions previously bound to the surface. Based on this, the formation of $Sr(OH)^+$ species at alkaline pH further contributes to adsorption through electrostatic interactions with the negatively charged surface [54].

- The interval of pH 3-6, the Ca-Alg-AO adsorbent, which contains amidoxime and carboxyl groups, adsorbs metal ions through ion exchange and the formation of metal-ligand complexes on its surface (Figure 9a).
- The interval of pH 6 - 7, For oxidized Ca-Alg-AO, ion exchange plays a more significant role in adsorption. Dissociated carboxylate groups ($-COO^-$) facilitate the replacement of Ca^{2+} or H^+ ions on the adsorbent surface with Sr^{2+} ions from the solution. This process operates synergistically with the formation of metal-ligand complexes, in which Sr^{2+} ions coordinate with the active functional groups. Furthermore, the species of Sr(II), $Sr(OH)_2$, $Sr(OH)^+$, and $Sr(OH)_3^-$ begin to form in the solution (Figure 9b).
- At higher pH levels (pH > 7), Sr(II) adsorption onto oxidized Ca-Alg-AO is dominated by a combination of ion exchange and complexation mechanisms ((Figure 9c). The deprotonation of carboxylate and amidoxime groups increases the negative surface charge, providing more binding sites for Sr^{2+} ions. Additionally, the formation of $Sr(OH)^+$ species at alkaline pH contributes to adsorption through electrostatic interactions. However, at very high pH, the formation of $Sr(OH)_2$ precipitates on the adsorbent surface or in the solution may enhance the removal of Sr^{2+}, although not through direct adsorption mechanisms.

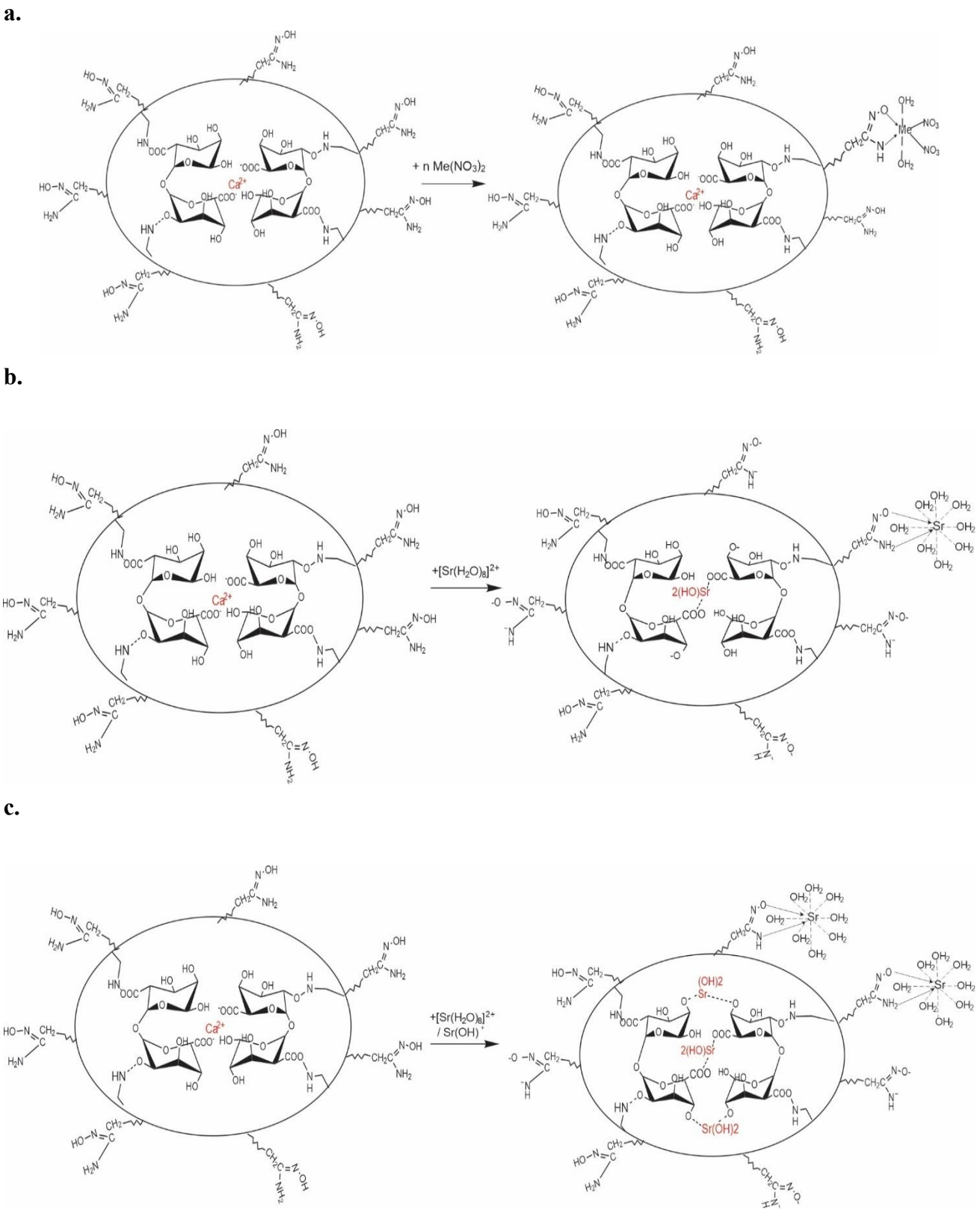

Figure 9. Schematic presentation of the adsorption of metal ions on Ca-Alg-AO by complexation (a), by ion exchange and the formation of metal–ligand complexes on the surface (b), and by exchange and complexation (c).

3.2.6. Adsorbent reusability

Reusability is a critical parameter to consider for practical and commercial applications of adsorbents, as it significantly reduces process costs. An ideal adsorbent should be easily regenerable and reusable. Acidic or alkaline treatments are commonly employed for regenerating adsorbents, but these methods can potentially damage the adsorbent structure, leading to a reduction in adsorption efficiency after each regeneration cycle. Therefore, careful selection of the acid/alkali type and its concentration is crucial [55,56].

In this study (Figure 10), the adsorption performance of Ca-Alg-AO beads for Sr(II) was evaluated over five consecutive regeneration cycles. After Sr(II) adsorption, the loaded adsorbent was treated with 1M HNO_3 for 30 minutes at room temperature, followed by thorough washing and drying at 60 °C. The regenerated adsorbent was reused for subsequent adsorption tests. Figure 12 illustrates the effect of regeneration cycles on Sr(II) adsorption capacity. The first cycle achieved the highest removal efficiency (77.55%). In the second and third cycles, a slight decline in adsorption capacity was observed (5.35% and 5.3%, respectively), but it increased again in the fourth and fifth cycles. The decrease in adsorption during the second and third cycles can be caused structural or surface chemical changes in the adsorbent. The acidic regeneration process might partially modify the functional groups responsible for binding Sr(II), such as carboxylate or amidoxime groups, by altering their accessibility or reactivity. Despite these minor decreases, Ca-Alg-AO beads demonstrated strong reusability, maintaining Sr(II) removal efficiency >70% even after five cycles. This highlights the robustness of the adsorbent for practical applications.

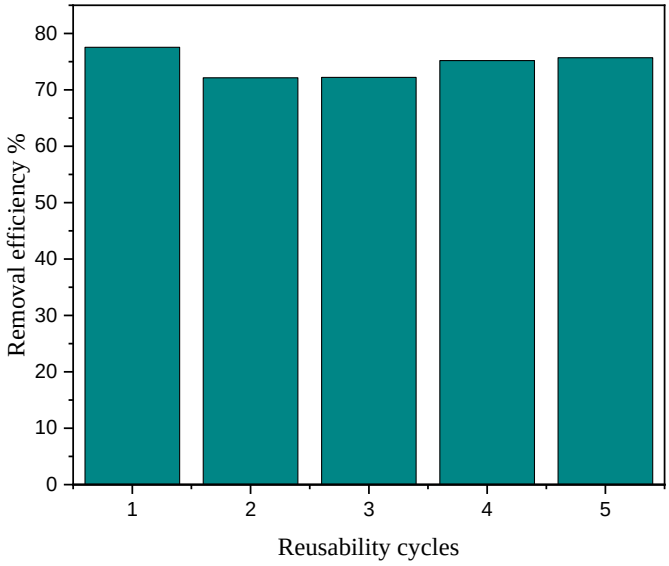

Figure 10. Reusability of the Ca-Alg-AO for the removal of Sr(II).

After undergoing five cycles of adsorption and regeneration, the Ca-Alg-AO beads retained 75.7% of their initial adsorption capacity, indicating exceptional durability of the developed adsorbent. Furthermore, the findings revealed only a minor decrease in the adsorbent's performance, with a slight reduction. This decline in efficiency can be attributed to a reduction in the number of active sites on the Ca-Alg-AO surface. Notably, the loss in adsorption capacity was less than 4%, demonstrating the

material's excellent recyclability and its ability to maintain consistent regeneration efficiency over repeated cycles. These results confirm the successful regeneration of Ca-Alg-AO beads. Consequently, the stability exhibited by Ca-Alg-AO after multiple reuse cycles highlights its potential as an effective and cost-efficient adsorbent for the removal of Sr(II) from contaminated solutions.

4. Conclusions

The Ca-Alg-AO beads, synthesized from natural coral skeleton waste and functionalized with amidoxime acid-base groups, exhibited effective adsorption properties for Sr(II). Characterization confirmed successful synthesis, evidenced by the presence of functional groups such as ACN at 2251 cm^{-1}, C=N stretching vibration at 1651 cm^{-1}, and N–O vibration at 939 cm^{-1}. TGA analysis revealed final degradation between 282.2 and 652.1 °C, involving chain scission and monomer release, with a weight loss of 17.1%. XRF analysis showed an increase in calcium purity from 94.63% to 94.76%. SEM analysis highlighted improved structural density on the adsorbent surface. In aqueous solutions, Ca-Alg-AO achieved a high Sr(II) adsorption efficiency of 84.8 ± 1% and an adsorption capacity of 13.58 mg/g (adsorbent dose: 0.025 g; volume: 0.02 L; reaction time: 120 min; temperature: 27 °C; rotational speed:130 rpm). Kinetic data followed the pseudo-second-order model (R^2 = 0.992), while adsorption isotherms aligned better with the Langmuir model (R^2 = 0.999). Thermodynamic studies confirmed an exothermic and spontaneous adsorption process driven by entropy mechanisms.

In seawater, the adsorption capacity decreased to 4.02 mg/g, primarily due to ion competition and Sr(II) speciation changes. At lower pH (3–6), Sr^{2+} adsorption involved ion exchange and metal-ligand complexation via amidoxime and carboxyl groups. As the pH increased to 6–7, ion exchange became dominant, with dissociated carboxylate groups replacing Ca^{2+} or H^+ ions, supported by $Sr(OH)_2$ and $Sr(OH)^+$ species formation. At higher pH (>7), adsorption was driven by functional group deprotonation, increasing negative surface charge and enhancing electrostatic interactions and complexation. However, excessive pH led to $Sr(OH)_2$ precipitation, contributing to Sr^{2+} removal without direct adsorption. Reusability tests showed that after five adsorption-regeneration cycles, Ca-Alg-AO retained 75.7% of its initial adsorption capacity, demonstrating exceptional durability of the developed adsorbent.

Authors' contributions

Conceptualization: Alif Alfarisyi Syah, Anugrah Ricky Wijaya; Data curation: Anugrah Ricky Wijaya, Alif Alfarisyi Syah, Intan Ainul Malik. Formal Analysis: Alif Alfarisyi Syah, Anugrah Ricky Wijaya. Funding: Thesis Research Grant DRTPM 2024, No. 0459/E5/PG.02.00/2024 ; Investigation: Alif Alfarisyi Syah, Anugrah Ricky Wijaya, Intan Ainul Malik; Methodology: Alif Alfarisyi Syah, Anugrah Ricky Wijaya; Project administration: Dewinta Yuka; Resources: Alif Alfarisyi Syah, Anugrah Ricky Wijaya; Software: Alif Alfarisyi Syah; Supervision: Anugrah Ricky Wijaya; Validation: Anugrah Ricky Wijaya; Visualization: Alif Alfarisyi Syah; Writing–original draft: Alif Alfarisyi Syah, Anugrah Ricky Wijaya; Writing –review & editing: Alif Alfarisyi Syah, Anugrah Ricky Wijaya.

Use of AI tools declaration

The authors declare that no Artificial Intelligence (AI) tools were used in the initial creation of this article.

Acknowledgments

The authors would like to express their deepest gratitude to the Directorate of Research, Technology, and Community Service (DRTPM) for funding this research through the 2024 Thesis Research Grant, No. 0459/E5/PG.02.00/2024. This support has been invaluable in enabling the successful execution of this study. Additionally, we extend our appreciation to all individuals and institutions who contributed to the research process, providing essential facilities, guidance, and collaboration.

Conflict of interests

The authors state that there are no conflicts of interest for this project.

References

1. Bardi U (2010) Extracting minerals from seawater: an energy analysis. *Sustainability* 2: 980-992. https://doi.org/10.3390/su2040980
2. Yao Y, Gao B, Zhang M, et al. (2012) Effect of biochar amendment on sorption and leaching of nitrate, ammonium, and phosphate in a sandy soil. *Chemosphere* 89: 1467-1471. https://doi.org/10.1016/j.chemosphere.2012.06.002
3. Angino E E, Billings G K, Andersen N (1966) Observed variations in the strontium concentration of sea water. *Chemical Geology* 1: 145-153. https://doi.org/10.1016/0009-2541(66)90013-1
4. Nanlohy F, Wijaya A R, Semedi B, et al. (2023) Adsorption of strontium (Sr2+) in seawater using adsorbent Fe3O4/MnO2/fulvic acid nanocomposite[C]//AIP Conference Proceedings. AIP Publishing 2634(1). https://doi.org/10.1063/5.0112262
5. Ryu J, Hong J, Park I S, et al. (2020) Recovery of strontium (Sr2+) from seawater using a hierarchically structured MnO2/C/Fe3O4 magnetic nanocomposite. *Hydrometallurgy* 191: 105224. https://doi.org/10.1016/j.hydromet.2019.105224
6. Hong H J, Park I S, Ryu T, et al. (2018) Demonstration of seawater strontium (Sr (II)) extraction and enrichment by a biosorption technique through continuous column operation. *Industrial & Engineering Chemistry Research* 57: 12909-12915. https://doi.org/10.1021/acs.iecr.8b02895
7. Jeong S K, Ju C S (2002) Extraction of strontium ion from sea water by contained liquid membrane permeator. *Korean Journal of Chemical Engineering* 19: 93-98. https://doi.org/10.1007/BF02706880
8. Nagaoka M, Yokoyama H, Fujita H, et al. (2015) Spatial distribution of radionuclides in seabed sediments off Ibaraki coast after the Fukushima Daiichi Nuclear Power Plant accident *J Radioanal Nucl Chem* 303: 1305–1308. https://doi.org/10.1007/s10967-014-3633-9

9. Shozugawa K, Riebe B, Walther C, et al. (2016) Fukushima-derived radionuclides in sediments of the Japanese Pacific Ocean coast and various Japanese water samples (seawater, tap water, and coolant water of Fukushima Daiichi reactor unit. *J Radioanal Nucl Chem* 307: 1787–1793. https://doi.org/10.1007/s10967-015-4386-9
10. Sachse A, Merceille A, Barré Y, et al. (2012) Macroporous LTA-monoliths for in-flow removal of radioactive strontium from aqueous effluents: Application to the case of Fukushima. *Microporous Mesoporous Mater* 164: 251–258. https://doi.org/10.1016/j.micromeso.2012.07.019
11. Hong H J, Ryu J, Park I S, et al. (2016) Investigation of the strontium (Sr(II)) adsorption of an alginate microsphere as a low-cost adsorbent for removal and recovery from seawater. *J Environ Manage* 165: 263–270. https://doi.org/10.1016/j.jenvman.2015.09.040
12. Zhao J, Liu J, Li N, et al. (2016) Highly efficient removal of bivalent heavy metals from aqueous systems by magnetic porous Fe3O4-MnO2: Adsorption behavior and process study. *Chem Eng J* 304: 737–746. https://doi.org/10.1016/j.cej.2016.07.003
13. Marinin D V, Brown G N (2000) Studies of sorbent/ion-exchange materials for the removal of radioactive strontium from liquid radioactive waste and high hardness groundwaters *Waste Manag* 20: 545–553. https://doi.org/10.1016/S0956-053X(00)00017-9
14. Rane A V, Kanny K, Abitha V K, et al. (2018) Methods for synthesis of nanoparticles and fabrication of nanocomposites[M]//Synthesis of inorganic nanomaterials. *Woodhead publishing* 2018: 121-139. https://doi.org/10.1016/B978-0-08-101975-7.00005-1
15. Wijaya A R, Syah A A, Hana D C, et al. (2024) Addition of chitosan to Calcium-Alginate Membranes for Seawater NaCl Adsorption. *AIMS Environ Sci* 11: 75–89. https://doi.org/10.3934/environsci.2024005
16. Fiol N, Poch J, Villaescusa I (2005) Grape stalks wastes encapsulated in calcium alginate beads for Cr(VI) removal from aqueous solutions. *Sep Sci Technol* 40: 1013–1028. https://doi.org/10.1081/SS-200048041
17. Gok C, Aytas S (2009) Biosorption of uranium(VI) from aqueous solution using calcium alginate beads. *J Hazard Mater* 168: 369–375. https://doi.org/10.1016/j.jhazmat.2009.02.063
18. Li X, Qi Y, Li Y, et al. (2013) Novel magnetic beads based on sodium alginate gel crosslinked by zirconium(IV) and their effective removal for Pb2+ in aqueous solutions by using a batch and continuous systems. *Bioresour Technol* 142: 611–619. https://doi.org/10.1016/j.biortech.2013.05.081
19. Hu S, Lin X, Zhang Y, et al. (2017) Preparation and application of alginate-Ca/attapulgite clay core/shell particle for the removal of uranium from aqueous solution. *J Radioanal Nucl Chem* 314: 307–319. https://doi.org/10.1007/s10967-017-5427-3
20. Wijaya A R, Syah A A, Hana D C, et al. (2024) Addition of chitosan to Calcium-Alginate Membranes for Seawater NaCl Adsorption. *AIMS Environ Sci* 11: 75–89. https://doi.org/10.3934/environsci.2024005
21. Nakayama R, Takamatsu Y, Namiki N (2020) Multiphase calcium alginate membrane composited with cellulose nanofibers for selective mass transfer. *SN Appl Sci* 2: 1–7. https://doi.org/10.1007/s42452-020-03532-1

22. Chen J H, Li G P, Liu Q L, et al. (2010) Cr(III) ionic imprinted polyvinyl alcohol/sodium alginate (PVA/SA) porous composite membranes for selective adsorption of Cr(III) ions. *Chem Eng J* 165: 465–473. https://doi.org/10.1016/j.cej.2010.09.034
23. Yang M, Xia Y, Wang Y, et al. (2016) Preparation and property investigation of crosslinked alginate/silicon dioxide nanocomposite films. *J Appl Polym Sci* 133: 22. https://doi.org/10.1002/app.43489
24. Manez K S, Husain S, Ferse S C A, et al. (2012) Water scarcity in the Spermonde Archipelago, Sulawesi, Indonesia: Past, present and future. *Environ Sci Policy* 23: 74–84. https://doi.org/10.1016/j.envsci.2012.07.004
25. Li L, Fang Y, Vreeker R, et al. (2007) Reexamining the egg-box model in calcium - Alginate gels with X-ray diffraction. *Biomacromolecules* 8: 464–468. https://doi.org/10.1021/bm060550a
26. Kamila N S, Syah A A, Wijaya A R (2024) Application of Silica from Beach Sand in the Synthesis of Calcium-Alginate-Silica as Adsorbent of Na + and Cl - Ions. *E3S Web Conf* 481: 03011. https://doi.org/10.1051/e3sconf/202448103011
27. Syah A A, Wijaya A R, Kusumaningrum I K (2024) Preparation and development of amidoxime-modified Fe3O4/SiO2 core-shell magnetic microspheres for enhancing U(VI) adsorption efficiency from seawater. *Aims Environ Sci* 11: 21–37. https://doi.org/10.3934/environsci.2024002
28. Gao B, Gao Y, Li Y (2010) Preparation and chelation adsorption property of composite chelating material poly(amidoxime)/SiO2 towards heavy metal ions. *Chem Eng J* 158: 542–549. https://doi.org/10.1016/j.cej.2010.01.046
29. Zhao Y, Li J, Zhao L, et al. (2014) Synthesis of amidoxime-functionalized Fe3O4@SiO2 core-shell magnetic microspheres for highly efficient sorption of U(VI). *Chem Eng J* 235: 275–283. https://doi.org/10.1016/j.cej.2013.09.034
30. Wei Y, Salih K A M, Lu S, et al. (2019) Amidoxime functionalization of algal/polyethyleneimine beads for the sorption of Sr(II) from aqueous solutions. *Molecules* 24. https://doi.org/10.3390/molecules24213893
31. Putra H F S, Syah A A, Wijaya A R (2024) Application of Calcium Alginate Products for Seawater Desalination Process. 03010. https://doi.org/10.1051/e3sconf/202448103010
32. Wu F C, Tseng R L, Juang R S (2009) Initial behavior of intraparticle diffusion model used in the description of adsorption kinetics. *Chem Eng J* 153: 1–8. https://doi.org/10.1016/j.cej.2009.04.042
33. Skwarek E, Gładysz-Płaska A, Choromańska J B, et al. (209) Adsorption of uranium ions on nano-hydroxyapatite and modified by Ca and Ag ions. *Adsorption* 25: 639–647. https://doi.org/10.1007/s10450-019-00063-z
34. Ou M, Li W, Huang Z, et al. (2023) Highly efficient extraction of uranium (VI) from seawater by Polyamidoxime/polyethleneimine sponge. *Sep Purif Technol* 331: 1–34. https://doi.org/10.1016/j.seppur.2023.125721
35. Wang D, Song J, Lin S, et al. (2019) A Marine-Inspired Hybrid Sponge for Highly Efficient Uranium Extraction from Seawater. *Adv Funct Mater* 29: 1–12. https://doi.org/10.1002/adfm.201901009

36. Jeong C, Kim S, Lee C, et al. (2020) Changes in the physical properties of calcium alginate gel beads under a wide range of gelation temperature conditions. *Foods* 9. https://doi.org/10.3390/foods9020180
37. Kim S, Jeong C, Cho S, et al. (2019) Effects of thermal treatment on the physical properties of edible calcium alginate gel beads: Response surface methodological approach. *Foods* 8. https://doi.org/10.3390/foods8110578
38. Zhao W, Qi Y, Wang Y, et al. (2018) Morphology and thermal properties of calcium alginate/reduced graphene oxide composites. *Polymers* 10: 1–11. https://doi.org/10.3390/polym10090990
39. P. M. V Raja, A. R. Barron (1934) Physical methods in chemistry *Nature* 134: 366–367. https://doi.org/10.1002/jctb.5000533702
40. Ablouh E, Hanani Z, Eladlani N, et al. (2019) Chitosan microspheres/sodium alginate hybrid beads: An efficient green adsorbent for heavy metals removal from aqueous solutions. *Sustain Environ Res*1: 1–11. https://doi.org/10.1186/s42834-019-0004-9
41. Dragan E S, Humelnicu D, Ignat M, et al. (2020) Superadsorbents for Strontium and Cesium Removal Enriched in Amidoxime by a Homo-IPN Strategy Connected with Porous Silica Texture. *ACS Appl Mater Interfaces* 12: 44622–44638. https://doi.org/10.1021/acsami.0c10983
42. Jamshidi A, Rezaei S, Hassani G, et al. (2021) Optimization and modeling of ammonia removal from aqueous solutions by using adsorption on single-walled carbon nanotubes," *J. Eng. Technol. Sci.*, vol. 53, no. 3, 2021, https://doi.org/10.5614/j.eng.technol.sci.2021.53.3.9
43. Sharifnia S, Khadivi M A, Shojaeimehr T, et al. (2016) Characterization, isotherm and kinetic studies for ammonium ion adsorption by light expanded clay aggregate (LECA). *J Saudi Chem Soc* 20: S342–S351. https://doi.org/10.1016/j.jscs.2012.12.003
44. Syafiuddin A, Salmiati S, Jonbi J, et al. (2018) Application of the kinetic and isotherm models for better understanding of the behaviors of silver nanoparticles adsorption onto different adsorbents. *J Environ Manage* 218: 59–70. https://doi.org/10.1016/j.jenvman.2018.03.066
45. Utomo S B, Jumina J, Siswanta D, et al. (2012) Kinetics and equilibrium model of Pb(II) and Cd(II) adsorption onto tetrakis-thiomethyl-C-4-methoxyphenylcalix[4]resorcinarene. *Indones J Chem* 12: 49–56. https://doi.org/10.22146/ijc.21371
46. Sadeghi S, Azhdari H, Arabi H, et al. (2012) Surface modified magnetic Fe 3O 4 nanoparticles as a selective sorbent for solid phase extraction of uranyl ions from water samples. *J Hazard Mater* 215–216: 208–216. https://doi.org/10.1016/j.jhazmat.2012.02.054
47. Galamini G, Ferretti G, Medoro V, et al. (2020) Isotherms, kinetics, and thermodynamics of nh4 + adsorption in raw liquid manure by using natural chabazite zeolite-rich tuff. *Water Switz* 12: 1–16. https://doi.org/10.3390/w12102944
48. Uğurlu M, Gürses A, Açıkyıldız M (2008) Comparison of textile dyeing effluent adsorption on commercial activated carbon and activated carbon prepared from olive stone by ZnCl2 activation. *Microporous Mesoporous Mater* 111: 228–235. https://doi.org/10.1016/j.micromeso.2007.07.034
49. Uğurlu M, Karaoğlu M H (2011) Adsorption of ammonium from an aqueous solution by fly ash and sepiolite: Isotherm, kinetic and thermodynamic analysis. *Microporous Mesoporous Mater* 139: 173–178. https://doi.org/10.1016/j.micromeso.2010.10.039

50. Ghaemi A, Torab-Mostaedi M, Ghannadi-Maragheh M (2011) Characterizations of strontium(II) and barium(II) adsorption from aqueous solutions using dolomite powder. *J Hazard Mater* 190: 916–921. https://doi.org/10.1016/j.jhazmat.2011.04.006
51. Ghaeni N, Taleshi M S, Elmi F (2019) Removal and recovery of strontium (Sr(II))from seawater by Fe3O4/MnO2/fulvic acid nanocomposite. *Mar Chem* 213: 33–39. https://doi.org/10.1016/j.marchem.2019.05.003
52. Persson I (2010) Hydrated metal ions in aqueous solution: How regular are their structures? *Pure Appl Chem* 82: 1901–1917. https://doi.org/10.1351/PAC-CON-09-10-22
53. Hasan S, Iasir A R M, Ghosh T K, et al. (2019) Characterization and adsorption behavior of strontium from aqueous solutions onto chitosan-fuller's earth beads. *Healthc Switz* 7. https://doi.org/10.3390/healthcare7010052
54. Ceban G I, Nastas R (2023) Some considerations of nitrite ions adsorption on activated carbons. The suggested mechanisms. 16–16. https://doi.org/10.19261/enece.2022.ab07
55. Zaman H G, Baloo L, Kutty S R, et al. (2023) Post Synthetic Modification of NH2-(Zr-MOF) via Rapid Microwave-promoted Synthesis for Effective Adsorption of Pb(II) and Cd(II). *Arab J Chem* 16: 104122. https://doi.org/10.1016/j.arabjc.2022.104122
56. Birniwa A H, Mohammad R E A, Ali M, et al. (2022) Synthesis of Gum Arabic Magnetic Nanoparticles for Adsorptive Removal of Ciprofloxacin: Equilibrium, Kinetic, Thermodynamics Studies, and Optimization by Response Surface Methodology. *Separations* 9. https://doi.org/10.3390/separations9100322

AIMS Press